

Universal Cell Embeddings: A Foundation Model for Cell Biology

Yanay Rosen^{1,*}, Yusuf Roohani^{2,*}, Ayush Agarwal¹, Leon Samotorčan¹,
Tabula Sapiens Consortium³, Stephen R. Quake^{4,5,6,†}, Jure Leskovec^{1,†}

¹ Department of Computer Science, Stanford University, Stanford, CA, USA

² Department of Biomedical Data Science, Stanford University, Stanford, CA, USA

³ Chan Zuckerberg BioHub, San Francisco, CA, USA

⁴ Department of Bioengineering, Stanford University, Stanford, CA, USA

⁵ Department of Applied Physics, Stanford University, Stanford, CA, USA

⁶ Chan Zuckerberg Initiative, Redwood City, CA, USA

†Corresponding author. Email: jure@cs.stanford.edu, quake@stanford.edu

*These authors contributed equally

Abstract

Developing a universal representation of cells which encompasses the tremendous molecular diversity of cell types within the human body and more generally, across species, would be transformative for cell biology. Recent work using single-cell transcriptomic approaches to create molecular definitions of cell types in the form of cell atlases has provided the necessary data for such an endeavor. Here, we present the Universal Cell Embedding (UCE) foundation model. UCE was trained on a corpus of cell atlas data from human and other species in a completely self-supervised way without any data annotations. UCE offers a unified biological latent space that can represent any cell, regardless of tissue or species. This universal cell embedding captures important biological variation despite the presence of experimental noise across diverse datasets. An important aspect of UCE's universality is that any new cell from any organism can be mapped to this embedding space with no additional data labeling,

25 **model training or fine-tuning. We applied UCE to create the Integrated Mega-scale Atlas,**
26 **embedding 36 million cells, with more than 1,000 uniquely named cell types, from hundreds**
27 **of experiments, dozens of tissues and eight species. We uncovered new insights about the or-**
28 **ganization of cell types and tissues within this universal cell embedding space, and leveraged**
29 **it to infer function of newly discovered cell types. UCE’s embedding space exhibits emergent**
30 **behavior, uncovering new biology that it was never explicitly trained for, such as identifying**
31 **developmental lineages and embedding data from novel species not included in the train-**
32 **ing set. Overall, by enabling a universal representation for every cell state and type, UCE**
33 **provides a valuable tool for analysis, annotation and hypothesis generation as the scale and**
34 **diversity of single cell datasets continues to grow.**

35 **Introduction**

36 Cells are the fundamental unit of life and biologists have long conceptualized cells as members
37 of different universal landscapes [1–4]. A notable example of this is the Waddington landscape,
38 which presents a theoretical framework for the developmental lineages of cells as they transition
39 from pluripotent stages such as stem cells to more terminally differentiated end points [5]. Broadly,
40 the field of cell biology has sought to map the range of phenotypes that cells might exhibit, their
41 interrelationships, and the shifts between these states during development and disease [6–10].

42 The substantial growth in the size of single-cell RNA sequencing (scRNA-seq) datasets
43 presents a fresh opportunity to revisit these questions. Detailed transcriptomic snapshots of cells
44 are now widely available from a range of timepoints, tissues, donors, and species [11–13]. These
45 rich, high-dimensional states are typically distilled into low-dimensional vectors or embeddings
46 to facilitate computational analysis [14, 15]. However, existing computational approaches strug-
47 gle to jointly analyze these diverse datasets. The unified representations they produce are often
48 unable to extend to new datasets due to species-specific constraints in their construction or the
49 presence of dataset-specific artifacts (or batch effects) which can obscure the underlying biologi-
50 cal signal [16, 17].

51 Some computational methods for scRNA-seq data have managed to overcome these limita-
52 tions, but at the cost of requiring model tuning for each new dataset, thus rendering the represen-
53 tations non-universal [15, 18, 19]. As a result, whenever a new experiment is performed and new
54 data is collected, it requires dedicated, resource-intensive data labeling and model training to per-
55 form even the most standard analyses, such as clustering or annotation. This process is both time
56 consuming and inefficient, and results in sub-optimal analyses based on small, limited and private
57 datasets.

58 Recent advances in the field of artificial intelligence have enabled general-purpose founda-
59 tion models (such as ChatGPT [20, 21], PaLM [22], Llama [23] and SAM [24]) that can learn
60 universal representations that are then applied to diverse downstream tasks and analyses. These
61 foundation models are not specifically trained for these downstream tasks, thus presenting clear
62 instances of emergent capabilities [25]. This foundation model strategy has also found valu-
63 able applications in biological contexts such as learning representations of protein and DNA se-
64 quences [26, 27]. While some recent work has applied foundation model architectures to single-cell
65 genomics data, the unique characteristics of these datasets necessitate a specialized modeling ap-
66 proach to fully realize their potential [28, 29]. Directly modeling gene expression as text in the

67 form of a sequence of genes is both inefficient from a learning perspective and often relies on
68 inaccurate biological assumptions.

69 Here, we present Universal Cell Embedding (UCE), a foundation model for single-cell gene
70 expression that is designed to address questions in cell and molecular biology. UCE is uniquely
71 able to generate representations of new single-cell gene expression datasets with no model fine-
72 tuning or retraining while still remaining robust to dataset and batch-specific artifacts. Moreover,
73 it does so while requiring no cell type annotation and no input dataset preprocessing, such as
74 gene selection. UCE can be applied to any set of genes from any species, even if they aren't
75 homologs of genes seen during training. UCE learns a universal representation of cell biology that
76 is intrinsically meaningful and can extend insights beyond the data that has been experimentally
77 observed. The representations learned by UCE display an emergent organization of cell types that
78 is consistent with known biology. These cell embeddings can be used to accurately predict cell
79 types with no additional model retraining, showing improved performance in dataset integration
80 against existing atlas-scale integration methods.

81 UCE presents a novel approach to analyzing cell states. It enables the mapping of new
82 data into a universal embedding space, already populated with annotated reference states. This
83 strategy addresses issues such as noisy measurements that limit data alignment across different
84 experiments, and reduces reliance on small sets of marker genes to translate insights across studies
85 [30]. UCE empowers researchers to utilize existing models on new data without needing data
86 labeling or model retraining. This can foster novel cross-dataset discoveries and overcome the
87 limitations currently faced when working with small, isolated datasets. For instance, a cell type
88 classifier trained to predict specific immune cell types can be seamlessly applied to a completely
89 new dataset. Thus, UCE offers a versatile, efficient, and broadly applicable framework for the
90 analysis of cell states.

91 **Results**

92 **A biologically-informed foundation model for single cell gene expression.**

93 Integrating single-cell RNA sequencing (scRNA-seq) datasets is challenging for two primary
94 reasons: scRNA-seq data does not always contain the same genes, or features, and those features
95 are plagued by dataset-specific experimental artifacts or batch effects, which means models have
96 to be built separately for each dataset. UCE overcomes these challenges by abstracting cells as

97 ‘bags of RNA’ [31]. UCE (Fig. 1a) converts the RNA gene expression of a single cell into an
98 expression weighted sample of its corresponding genes. Next, UCE represents the sample’s genes
99 by their protein products, using a large protein language model. This allows UCE to meaningfully
100 represent any gene, from any species, regardless of whether the species had appeared in the training
101 data. Finally, after incorporating additional metadata about genes’ chromosomal locations, this
102 representation is fed into a large transformer model [32]. UCE is able to map any cell, from any
103 tissue, or any species, into one shared universal space, with no additional training.

104 In particular, UCE takes as an input (1) scRNA-seq count data and (2) the corresponding
105 protein embeddings, generated by a large protein language model, ESM2 [33], for the genes in the
106 dataset. The ESM2 protein language model takes amino acid sequences as an input and produces
107 a numerical representation called a protein embedding. Given the expression count data for a cell,
108 UCE takes a weighted and normalized sample, with replacement, of the cell’s genes. This sample
109 can only contain genes which had non-zero expression, and can contain multiple copies of each
110 gene. These genes are then tokenized by converting them to the protein embedding representation
111 of the protein that they code for [34]. Genes belonging to the same chromosome are grouped
112 together by placing them in between special tokens and are then sorted by genomic location. A
113 special token representing the entire cell, the ‘CLS’ token, is appended to the beginning of the cell
114 representation [35]. This combined representation is passed into a transformer neural network. The
115 embedding of a cell is taken as the embedding of the CLS token at the final layer of the transformer
116 (Fig. 1a).

117 UCE is trained in a completely self-supervised manner, and thus does not make use of any
118 cell type or dataset-based annotations. In particular, during training, a random subset (20%) of
119 genes that were expressed are masked before sampling. These expressed genes are combined
120 with a random subset of genes which had zero expression (non-expressed genes) to form a set of
121 query genes. Each of these query genes’ protein embedding tokens is combined with the UCE
122 embedding of the cell they were generated from, and this joint embedding is passed into a fully
123 connected neural network that predicts if that gene was expressed.

124 UCE is a 33 layer model consisting of over 650 million parameters. UCE was trained across
125 more than 300 datasets that are largely collected from the CellXGene corpus [36] consisting of
126 over 36 million cells, for 40 days across 24 A100 80GB GPUs (Methods, Extended Data Table

127 2, Supplementary Table 2). The model's weights and implementation are freely available and the
128 model will be hosted as an openly available resource for the research community to run inference
129 on new datasets.

130 **UCE creates an Integrated Mega-scale Atlas (IMA) of 36 million cells.**

131 We apply UCE to generate an Integrated Mega-scale Atlas (IMA) of 36 million cells sam-
132 pled from diverse biological conditions, demonstrating the emergent organization of UCE cell
133 representations (Fig. 1b). We find that cells within the UCE space naturally cluster by biological
134 conditions like cell type, while mixing among experimental conditions like batch (Fig. 1b). Since
135 UCE is trained in a self-supervised manner, this organization represents an emergent behavior of
136 the model. The IMA contains numerous cell type alignments, across tissues and species.

137 To investigate the emergent organization of the IMA, we inspect how tissue residency can
138 influence the state of cell types. Although macrophages found in different tissues are characterized
139 by diverse transcriptional identities [37], they align closely in the UCE space (Extended Data Table
140 1). For the purpose of our analysis below, we first determine the central location of each cell type
141 and tissue combination in the IMA space, by averaging the UCE embeddings of the cells from that
142 combination, creating a tissue and cell type 'centroid'.

143 Cells in the IMA have been pre-labeled by their cell type. As these labels were never used
144 for training the UCE model, we use them to validate the quality of the learned representation.
145 For example, in the IMA, human macrophages are found in 73 different tissues and among these
146 tissues, 72% (53) of tissue-specific macrophage centroids were embedded closest to a macrophage
147 centroid from another tissue. Considering the 3 nearest centroids increases this percentage to 93%
148 (Extended Data Table 1). Similar cross-tissue homogeneity can also be identified in other prolific

149 cell types, like endothelial cells or neurons. This demonstrates that UCE, without any explicit
150 training or labels, identifies that macrophages have a unique cellular identity that is shared across
151 tissues. More broadly, it is an example of UCE’s emergent organization that is consistent with
152 known biology even though not explicitly trained for.

153 **UCE embeds new datasets without additional model training.**

154 We evaluated the universality of UCE representations by directly mapping new datasets
155 which were not part of the training set into the embedding, without any additional training or
156 refinement of the UCE model. This is referred to as a ‘zero-shot’ capability, since the model was
157 never trained on any samples from the new dataset (Fig. 2a) . While a variety of deep learning
158 models have been proposed for this task, we choose to compare the performance of UCE to other
159 self-supervised transformer-based methods. This is because they do not rely on cell type annota-
160 tion, are trained on large datasets, have high model capacity, and can be run in a zero-shot setting.

161 In particular, we compare against Geneformer [28] and scGPT [29], both of which represent cells
162 using ordered lists of gene tokens.

163 We assess the performance of these methods on a completely new and yet unreleased dataset
164 (as of the publication of this manuscript), Tabula Sapiens v2, which contains diverse human data
165 from 581,430 cells, 27 tissues, 167 batches and 162 unique cell types. We use established metrics
166 for embedding quality that measure the conservation of cell type information and the correction
167 of batch effects (Methods). We compared several methods and found that UCE substantially out-
168 performs the next best method Geneformer by 9.0% on overall score, 10.6% on biological conser-
169 vation score, and 7.4% on batch correction score (Supplementary Table 1). To comprehensively
170 assess the value of these zero-shot embeddings, we also compare UCE to fine-tuned methods that

171 are conventionally used for this task. Notably, UCE even performs slightly better than non-zero-
172 shot methods that require dataset-specific training: scVI [15] and scArches [18].

173 We also investigate the Tabula Sapiens v1 [11] (which was part of the training set) and v2
174 embeddings of each model visually by creating UMAP embeddings (Fig. 2b). UCE embeddings
175 distinctly separate cell types more effectively than other methods tested in zero-shot. Even though
176 UCE is not trained on the Tabula Sapiens v2 dataset, its embeddings more closely resemble those of
177 fine-tuned methods, which are directly trained on it. Moreover, cell types align correctly regardless
178 of whether the data was drawn from new donors or previously seen ones (Supplementary Fig. 1).

179 For all cell types in Tabula Sapiens v2, we calculate the silhouette width score of each zero-
180 shot embedding method. For 67% of cell types, UCE has the highest silhouette score of any
181 method. UCE outperforms Geneformer on 80% of cell types, tGPT on 73% of cell types, and
182 scGPT on 83% of cell types. Notably, UCE accurately embeds B cells, while Geneformer and
183 scGPT fail to do so (Supplementary Fig. 2a). In Tabula Sapiens v2, the silhouette width score of
184 B cells is 93% higher in UCE versus scGPT and 25% higher versus Geneformer. Additionally, B
185 cells within the UCE embedding space can be accurately mapped to an existing reference. We train
186 a simple logistic classifier on the UCE embeddings of the Immune Cell Atlas [38], and then apply
187 the classifier to B cell embeddings from Tabula Sapiens v2. This classifier accurately classifies the
188 Tabula Sapiens v2 cells as memory and naive B cells (Supplementary Fig. 2b), which is confirmed
189 with marker gene analysis (Supplementary Fig. 2c). Overall, these results illustrate that UCE has
190 the unique capability to meaningfully integrate new, previously unseen datasets into a universal
191 cell representation space with no additional model training.

192 **UCE embeds diverse cell types from organisms that were not part of the training data.**

193 UCE is also able to align datasets from novel species without additional model training. This

194 is due to the fact that UCE is not dependent on any particular genome—each gene of interest is

195 translated to a corresponding protein sequence, which is then embedded in a universal protein

196 space. The representation in this space is independent of species and importantly does not require

197 any judgment about whether particular pairs of genes are homologs or not. Since UCE can analyze

198 cell atlas data from distinct species that were not part of the training set, the extent to which it

199 succeeds in this task is a stringent test of whether UCE displays emergent behavior.

200 UCE’s training data is composed of datasets from eight species: human, mouse, mouse

201 lemur, zebrafish, pig, rhesus macaque, crab eating macaque and western clawed frog. We apply

202 UCE to embed datasets from three novel species that were not included in the training set. For each

203 species, we generate a zero-shot embedding and then determine the nearest cell type centroid from

204 the IMA for each of the dataset’s existing annotated cell types. For all three species we observed

205 very high agreement between independent annotations of the novel species’ data and the nearest

206 cell type centroids in the IMA.

207 Within a dataset of green monkey lymph node and lung cells [39], for 13 of the 17 cell

208 type centroids, the closest centroid from another species corresponds to the same cell type in the

209 green monkey. This match extends to all 17 centroids when considering the three nearest centroids

210 (Extended Data Table 1, Fig. 2c, 2d). Moreover, a population of lymph node cells that were

211 originally labelled as B cells, form a distinct cluster in UCE space (Supplementary Fig. 3b).

212 Differential expression analysis revealed that this cluster predominantly expresses a T cell marker,

213 *Cd3d* (Supplementary Fig. 3a, 3c).

214 In the case of naked mole rat spleen and circulating immune cells [40], for 17 out of 24 cell

215 types, the nearest cross species centroid matches the naked mole rat cell type (Extended Data Table
216 1, Supplementary Fig. 4b). In the case of chicken, we embed two distinct chicken datasets, chick
217 retina [41] and developing chick heart [42] (Supplementary Fig. 5a, 5b). Different eye-specific
218 neurons within the chick retina map to mouse lemur neurons, such as chick oligodendrocytes,
219 which are closest to mouse lemur oligodendrocytes (Extended Data Table 1). In chicken heart, 12
220 of 15 cell type centroids are matched within the nearest two cross species centroids (Extended Data
221 Table 1). No bird species were included when training UCE. Altogether, these results highlight that
222 UCE can be directly applied to investigate new and diverse datasets from previously unobserved
223 species.

224 **UCE learns a meaningful organization of cell types in previously unseen data.**

225 Moving beyond metrics focused on individual cell type clusters, we also examined the struc-
226 ture of the universal embedding space as a whole, through the relative positioning of different cells
227 within it. A meaningful arrangement of cell types emerges upon embedding all the cells from the
228 Tabula Sapiens v2 dataset from the lung tissue (Fig. 3a). Not only do distinct cell types like T cells,
229 monocytes and endothelial cells cluster together, but higher-level categories, such as immune cells
230 and epithelial cells, are also clearly distinguished.

231 To systematically assess this organization of cells within the embedding, we compared dis-
232 tances between pairs of cell types across all tissues in the embedding space to their distances in
233 the Cell Ontology tree [43] (Fig. 3b). We hypothesized that cells that are known to be similar
234 based on the cell ontology would likely also be closer together in the embedding space, and that
235 the degree of closeness would be correlated with ontological similarity. The results validate this re-
236 lationship: at each additional unit of separation between cell types in the cell ontology tree, there is

237 a significant increase in the embedding distance in UCE between those cell types. We consistently
238 observed this trend up to a distance of 5 hops in the ontology tree (Fig. 3b). However, beyond that,
239 the effect levels off (Supplementary Fig. 6). This is expected due to the curse of dimensionality
240 in high-dimensional spaces and the variability in the level of ontological refinement in different
241 branches of the ontology (Supplementary Note 3).

242 We also noted significant colocalization among cells originating from the same developmen-
243 tal lineages, in particular from the mesoderm, endoderm, and ectoderm germ layers. For Tabula
244 Sapiens v2, 90 out of 97 of the centroids for mesoderm-derived cell types had other mesoderm-
245 derived cell type centroids as their closest neighbors. A similar pattern was observed for 46 of the
246 56 endoderm-derived cell types and 22 of the 30 ectoderm-derived cell types (Supplementary Fig.
247 7a). A neural network classifier trained to predict the germ layer of origin for individual held-out
248 cell types using their universal embeddings showed an accuracy of over 80% (Supplementary Fig.
249 7b).

250 The accuracy of cell type organization in the Tabula Sapiens v2 lung dataset was evaluated by
251 comparing it with other lung datasets in the IMA (Fig. 3c, Supplementary Fig. 8). Four different
252 endothelial cell subtypes are observed to map correctly to their corresponding counterparts in the
253 IMA. Similarly, lung ciliated cells correctly map to their counterpart in the larger corpus despite
254 the presence of four different ciliated cell subtypes (Fig. 3c). Further analysis of the alignment of
255 cell type centroids between Tabula Sapiens v2 and the IMA across all tissues showed an average
256 correct alignment of 56% for each tissue, as detailed in the Methods section. This alignment, based
257 on the three nearest neighbor cell type centroids, is 60% more accurate compared to that measured
258 in the original gene expression space (Fig. 3d). When focusing on the single nearest centroid, the

259 alignment accuracy improves by 93%. These results demonstrate that UCE can effectively learn a
260 universal representation of cell biology that not only enables discrimination between individual cell
261 types but also captures their relative similarities across scales with the potential to reveal deeper
262 insights into development and function.

263 **A workflow for decoding the function of newly discovered cell types.**

264 UCE's zero-shot embedding capabilities unlock novel computational analyses of scRNA-
265 seq data and aid in hypothesis generation. Beyond identifying novel cell type clusters, UCE differs
266 from other methods in that the same cell type can also be easily compared against all previously
267 assayed cells across tissues, disease states and species. Moreover, UCE is not biased in this process
268 by existing annotations, opening the door for discovery of novel function (Fig. 4a). With existing
269 fine tuning based methods, every searched dataset would need to be integrated, requiring repeated
270 model retraining. Thus, UCE enables a new workflow for scRNA-seq data analysis that performs
271 an unbiased search across the universe of cell biology.

272 We present an example of this analysis by using the recently identified kidney Norn cell as
273 a case study. The kidney Norn cell is the long-sought erythropoietin (*Epo*) producing cell in the
274 kidney, and is characterized as fibroblast-like. We perform a zero-shot embedding of mouse renal
275 cells from [44], which produces a cluster of cells corresponding to Norn cells (Fig. 4b).

276 Using a simple logistic classifier trained on the embedding of mouse renal cells, we identify
277 Norn cell clusters in many kidney datasets. Since this classifier takes universal cell embeddings
278 as an input, we can directly apply it to all 36 million cells in the IMA, in a manner unbiased
279 by cell type annotations ascribed by previous studies. We also confirm these cell's Norn identity
280 using marker gene analysis. Cells classified as Norn cells in the top 13 kidney datasets by Norn

281 abundancy demonstrate preferential expression of the Norn markers *Dcn*, *Lpar1*, *Colla1*, *Cxcl12*,
282 and *Cfh* (Extended Data Table 3). Notably, *Epo* transcripts, which are often missing from datasets
283 and lowly expressed, are not typically differentially expressed in these cells. *Cxcl14*, another
284 marker of Norn cells, displays mixed expression patterns in these predicted Norn cells (Fig. 4c).
285 The same pattern of marker gene expression is also found in cells from other tissues, including lung
286 and heart datasets (Fig. 4c). Additionally, these predicted cells also share a common set of genes
287 that are lowly expressed in mouse renal Norn cells (Supplementary Fig. 9). The tissues with the
288 highest number of predicted Norn cells were gonad, heart and lung. While *Epo* expression has been
289 previously observed in the heart and lung tissue, the mechanisms and cell types associated with
290 this expression, and their relation to kidney Norn cells have not been previously determined [45].
291 Overall, this demonstrates that UCE can serve as an unbiased tool for predicting the existence of
292 novel cell types.

293 **UCE helps interrogate alternate lung disease outcomes.**

294 Lastly, we apply UCE and our simple Norn cell classifier to investigate Norn cells in lung
295 diseases. We generate an embedding of lung cells sampled from patients with idiopathic pulmonary
296 fibrosis (IPF), chronic obstructive pulmonary disease (COPD), or patients from a control group
297 [46]. We identify Norn-like lung cells that preferentially express Norn markers in all three groups
298 (Fig. 4d).

299 For these Norn-like lung cells, we identify differences across disease groups (Fig. 4e). COPD
300 and IPF are both associated with elevated bloodstream *Epo*, but COPD has levels higher than
301 IPF. Additionally, in patients with IPF, secondary erythrocytosis is absent or reduced compared
302 to patients with COPD [47–49]. Given the identification of Norn-like cells in the lung, and Norn

303 cell's production of *Epo*, it is possible that this difference in disease prognosis could be related to
304 disease associated differences in Norn-like cells.

305 In COPD predicted Norn cells, there is a significantly greater ratio of *Epas1* : *Egln1* tran-
306 scripts (p=0.035) than in IPF predicted Norn cells (Fig. 4e). *Epas1* is a master regulator of *Epo*
307 transcription, which is degraded by the oxygen sensing enzyme encoded by *Egln1* [44]. Control
308 and COPD predicted Norn cells express genes (*Bgn*, *Crispld2*) involved in glycosaminoglycan
309 pathways at different levels than IPF predicted Norn cells [50,51]. IPF cells also have significantly
310 lower expression of *Il6st* than cells in control or COPD groups.

311 Taken as a whole, these results indicate that Norn-like cells may be found in other tissues
312 in the body, and may play a previously unidentified role in disease. UCE greatly facilitates an
313 analysis of this scale and diversity because it is a universal model.

314 Discussion

315 UCE is a single-cell foundation model that is built from the ground up to represent cell biology
316 across the wide array of single-cell datasets. We envision UCE as an embedding approach that
317 enables researchers to map any new data, including entire atlases, into an accurate, meaningful and
318 universal space. The embedding space that emerges from UCE is highly structured and diverse and
319 aligns cell types across tissues and species. Additionally, these cell types organize themselves in a
320 pattern that reflects existing biological knowledge.

321 The UCE model has broad implications for the creation of large foundation models for single
322 cell biology. For large foundation models to be truly useful for scientific discovery, they must have
323 unique qualities that distinguish them from existing methods. Zero-shot embeddings are one such
324 important capability because it enables an intrinsically meaningful representation that can extend

325 insights beyond the data that has already been observed and annotated experimentally. Our results
326 demonstrate that UCE can achieve such a generalizable representation across different datasets
327 while maintaining accuracy on individual datasets, comparable to methods that require retraining
328 for each specific dataset.

329 By building UCE, we enable new and novel analyses of scRNA-seq data. However, these
330 analyses and corresponding benchmarks are still far from perfect, as they are generally limited by a
331 focus on coarse cell type labels. To better understand single-cell foundation models, and especially
332 how they scale, new analyses and benchmarks that surpass this resolution limit must be developed.
333 For a precise representation of biology, models must incorporate core biological motivation. To
334 this end, we recognize that current scRNA-seq foundation models, including UCE, do not account
335 for any information contained in the raw RNA transcripts. By aligning these transcripts to the
336 reference genome, vital data on genetic variation and crucial RNA-splicing processes are discarded
337 [52]. Future single cell foundation models should seek to include this genomic precision at the
338 transcript level. As these models adopt more biologically-relevant features, they will increasingly
339 be able to simulate the biological processes of cells, leading to the creation of “Virtual Cells”.

340 In 2002, Nobel laureate Sydney Brenner identified many of the core motivations for the
341 creation of cell atlases and virtual cells. Virtual cells should be the goal of biological foundation
342 modeling, because cells are the “real units of function and structure in an organism” [53]. Brenner
343 also identified the need for such models to be computationally efficient, predictive, and able to
344 generate new cell types. We believe that UCE represents a significant advancement in the progress
345 towards a virtual cell. Through learning a universal representation of every cell state and type, we
346 expect that UCE will be a valuable tool for analysis, annotation and hypothesis generation as the

347 scale and diversity of single-cell datasets continues to grow.

348 Methods

349 Overview of UCE.

350 UCE (Universal Cell Embedding) is a machine learning model for mapping single-cell gene
351 expression profiles into a universal embedding space, denoted as \mathcal{U} . In this space, each cell c_i is
352 represented as a d_{emb} -dimensional vector, where $d_{emb} = 1280$.

353 The model takes as input a dataset \mathcal{D} with N cells $\{\mathbf{c}_i\}_{i=1}^N$. Cells in \mathcal{D} can be drawn from
354 one or more distinct scRNA-seq experiments. Each cell c_i in \mathcal{D} is described by a gene expression
355 vector $\mathbf{x}^i \in \mathbb{N}^{K_i}$, where K_i is the number of genes measured in c_i and can differ across \mathcal{D} . The gene
356 expression vectors $\mathbf{x}^i \in \mathbb{N}^{K_i}$ are not subset to those with high variance. UCE defines a function
357 $f_u : \{\mathbb{N}^{K_i} \rightarrow \mathbb{R}^{d_{emb}}\}_{i=1}^N$ that maps each gene expression vector \mathbf{x}^i to its cell embedding vector \mathbf{h}^i .

358 Model input: Gene representation.

359 The expression of gene g in cell c_i is denoted by x_g^i , where g represents any protein-coding
360 gene. The corresponding token embedding p_g is a pretrained embedding for the protein(s) encoded
361 by the gene g . These embeddings are derived from a pretrained protein language model that takes
362 an amino acid sequence as input and returns a d_p -dimensional embedding vector as output. To
363 create p_g , we take the average of all proteins coded by gene g . In the context of UCE, we can
364 formulate this as a dictionary that maps each gene g to a d_p -dimensional protein embedding vector.
365 Specifically, we employ the ESM2 model, which yields embeddings of size $d_p = 5120$ [33, 34].

366 Model input: Cell representation.

367 For each cell c_i in the input dataset \mathcal{D} , we identify two distinct sets of protein-coding genes:
368 the expressed genes G_i^+ and the non-expressed genes G_i^- . These sets are defined as follows:

$$G_i^+ = \{g \mid x_g^i > 0\} \quad (1)$$

$$G_i^- = \{g \mid x_g^i = 0\} \quad (2)$$

369 For producing the cell embedding, a multi-set of 1024 non-unique genes G_i^s are sampled
 370 from the expressed genes G_i^+ , with replacement. The probability of sampling a gene $g \in G_i^+$ is
 371 weighted by the log normalized expression of that gene, which can be formulated as:

$$P(g \mid c_i) = \frac{\log(x_g^i)}{\sum_{g \in G_i^+} \log(x_g^i)} \quad (3)$$

372 where x_g^i is the expression count of gene g in cell c_i , and the sum in the denominator is over
 373 all genes in G_i^+ .

374 Once the multi-set G_i^s is compiled for each cell c_i , we arrange the genes within each chro-
 375 mosome according to their genomic positions. Different chromosomes are specified using special
 376 chromosome start and end tokens. Start tokens are unique to each chromosome and species. Every
 377 chromosome group is combined into a single sequence, with chromosome order randomly deter-
 378 mined. A cell-level CLS token is appended to the start of the sequence. It is designed to capture
 379 the cell-level embedding upon training the model. The final sequence of genes ordered by genomic
 380 location and separated by chromosome is referred to as the cell sentence S_i for cell c_i .

381 **Transformer Architecture.**

382 Each cell sentence S_i is fed into a transformer that consists of n_{lay} layers. Each layer con-
 383 tains a multi-head self-attention mechanism with n_{head} attention heads and a feedforward network
 384 operating over a hidden space of dimensionality d_{hid} . We also initialize sinusoidally-varying po-

385 sitional embeddings. Gene token embeddings are compressed using a single layer MLP to d_{emb} -
386 dimensional vectors before passing through the transformer.

387 **Model output: Cell embedding.**

388 The final output from the model is the cell embedding vector $\mathbf{h}_{cell}^i \in \mathcal{U}$ which corresponds
389 to the d_{emb} -dimensional embedding of the *CLS* token in the final layer of the model following
390 decoding with an additional MLP.

391 **Model training: Cell representation.**

392 At the time of training, we generate a set $G_i^{M+} \subset G_i^+$ by randomly selecting a certain
393 percentage (r_{mask}) of genes from G_i^+ , without replacement. This set is used for computing the loss
394 during training, and is masked from the cell representation.

395 The probability of sampling a gene $g \in G_i^+ \setminus G_i^{M+}$ (Equation 3) is then updated to be:

$$P(g \mid c_i) = \frac{\log(x_k^i)}{\sum_{g \in G_i^+ \setminus G_i^{M+}} \log(x_j^i)}, \quad (4)$$

396 We also establish two additional gene sets to be used for loss computation: $G_i^{L+} \in G$ and
397 $G_i^{L-} \in G$. G_i^{L+} and G_i^{L-} are randomly selected from the masked set of expressed genes G_i^{M+} and
398 the set of unexpressed genes G_i^- respectively. Both G_i^{L+} and G_i^{L-} are of equal size, specifically
399 $N_{loss}/2$. In the case of G_i^{L-} , the sampling is done without replacement unless $|G_i^-| < N_{loss}/2$.
400 Similarly G_i^{L-} , is also sampled without replacement unless $|G_i^{M+}| < N_{loss}/2$. In this case, G_i^{M+}
401 is used as-is alongwith additional samples drawn with replacement from the full set of expressed
402 genes G_i^+ .

403 **Model training: Loss Function.**

404 To calculate the loss function for a given cell c_i , the cell embedding vector \mathbf{h}_{emb}^i is individu-

405 ally concatenated with every gene g within both G_i^{L+} and G_i^{L-} . These concatenated vectors then
 406 serve as input to a feedforward multilayer perceptron (MLP), which computes the probability that
 407 gene g is expressed within cell c_i .

408 \mathbf{h}_{cell}^i represents the embedding vector for cell c_i and p_g represents the token embedding for
 409 gene g . Then the concatenated vector \mathbf{z}_g^i that serves as input to the MLP for cell c_i and gene g is:

$$p_g' = \text{MLP}(p_g) \quad (5)$$

$$\mathbf{z}_g^i = [\mathbf{h}_{cell}^i || p_g'] \quad (6)$$

410 where $||$ denotes the concatenation operation and p_g' is the compressed protein embedding.
 411 The MLP then processes this concatenated input to produce the predicted probability that
 412 gene g is expressed:

$$p(y_g^i) = \text{MLP}(\mathbf{z}_g^i) \quad (7)$$

413 This probability is then used in the binary cross-entropy loss function. The true classification
 414 labels for each gene's expression status in cell c_i are represented by the vector \mathbf{y}^i . UCE is trained
 415 to accurately predict the expression of genes in G_i^{L+} and the lack of expression in G_i^{L-} . The model
 416 is trained using a binary cross-entropy loss, which is averaged across all N_{loss} genes and all N
 417 cells in the minibatch as follows:

$$L = -\frac{1}{N} \sum_{i=1}^N \frac{1}{N_{loss}} \sum_{j=1}^{N_{loss}} [y_j^i \log(p(y_j^i)) + (1 - y_j^i) \log(1 - p(y_j^i))] \quad (8)$$

418 For further details on hyperparameter choices please see Supplementary Table 2.

419 **Creating the IMA and dataset preprocessing.**

420 The Integrated Mega-scale Atlas (IMA) used to train UCE was created by combining scRNA-
421 seq datasets from multiple publicly available sources. The majority of IMA data (33.9 million cells
422 and 285 datasets) is human and mouse data downloaded from CZI Cell X Gene (CxG) Census [36]
423 version "2023-07-10" (July 10th, 2023). Duplicate cells were removed by selecting primary cells
424 only. The remainder of the IMA is composed of 2.3 million cells from 28 datasets, from eight
425 different species: human, mouse, zebrafish, rhesus macaque, crab-eating macaque, mouse lemur,
426 frog, and pig.

427 For datasets from the CxG Census, preprocessing only involved filtering cells by minimum
428 gene counts (200) and genes by a minimum cells count of 10. No highly variable gene selection
429 was applied. For datasets collected from other sources, preprocessing was not uniform.

430 For visualization of the IMA (Fig. 1b), predicting green monkey cell types (Fig. 2d), match-
431 ing new species centroids (Extended Data Table 1), and prediction of Norn-like cells (Fig. 4,
432 Supplementary Fig. 9) a representative sample of the IMA was used in place of the full 36 million
433 cells. This representative sample was used in order to speed up computationally intensive tasks like
434 UMAP calculation. The sample was created by randomly choosing 10,000 cells from each dataset,
435 without replacement. For datasets with fewer than 10,000 cells, the entire dataset was included. In
436 total, this representative sample has 2,969,114 cells. The average number of cells per dataset in the
437 sample is 9486. For visualization and centroid calculation, cell types in the sample were coarsened
438 by mapping them to a set of 51 coarse cell types.

439 **Model Evaluation.**

440 • **Zero-shot embedding quality and clustering** For evaluating the quality of embeddings, we

441 used metrics from the single-cell integration benchmark [16].

442 • **Cell type organization** For each cell type dendrogram the Euclidean distance was used to
443 perform hierarchical clustering across all cells.

444 • **Comparison to cell ontology** Here, we used the tree distance between any two cell types in
445 Cell Ontology [43]. To determine the Euclidean distance distribution, we sampled 100,000
446 random pairs of cells from Tabula Sapiens v2.

447 • **Zero-shot cell type alignment to IMA** For each cell type θ , a centroid was identified sepa-
448 rately for data from Tabula Sapiens v2 (TSv2) c_θ^T and from IMA c_θ^I . For each cell type that
449 is present in both TSv2 and the IMA, the 3 nearest neighbor cell type centroids \mathbf{N}_θ^T to the
450 centroid in Tabula Sapiens c_θ^T were identified. These neighbors could be either from Tabula
451 Sapiens or from the IMA.

452 If this set of neighbors \mathbf{N}_θ^T to the anchor centroid from TSv2 data c_θ^T contains the centroid
453 for the same cell type in IMA data c_θ^I , then this was counted as a correct match.

454 This analysis was performed per tissue, both in the UCE embedding space as well as in the
455 original expression space (after log-normalization). In case of the original data represen-
456 tation, the set of 5704 shared genes across all human datasets were used to represent each
457 cell.

458 **Differential expression analysis of predicted Norn cells.**

459 A logistic classifier was trained to predict cell types from UCE embeddings on mouse kidney
460 cells. This classifier was then applied to UCE embeddings from the representative sample of IMA
461 datasets. Datasets were then split by tissue, and the datasets with the most predicted norn cells in

462 each tissue were used for differential expression analysis. The top 13 kidney datasets, top 6 lung
463 and top 6 heart datasets were chosen.

464 For each individual (full) dataset, RNA counts were log normalized, and then differential ex-
465 pression was run using default settings as implemented in Scanpy [54], comparing predicted Norn
466 cells to all other cells in the dataset. The results of these differential expression tests were used
467 to determine the log fold change of marker genes in predicted Norn cells (Fig. 4c, Supplementary
468 Fig. 9).

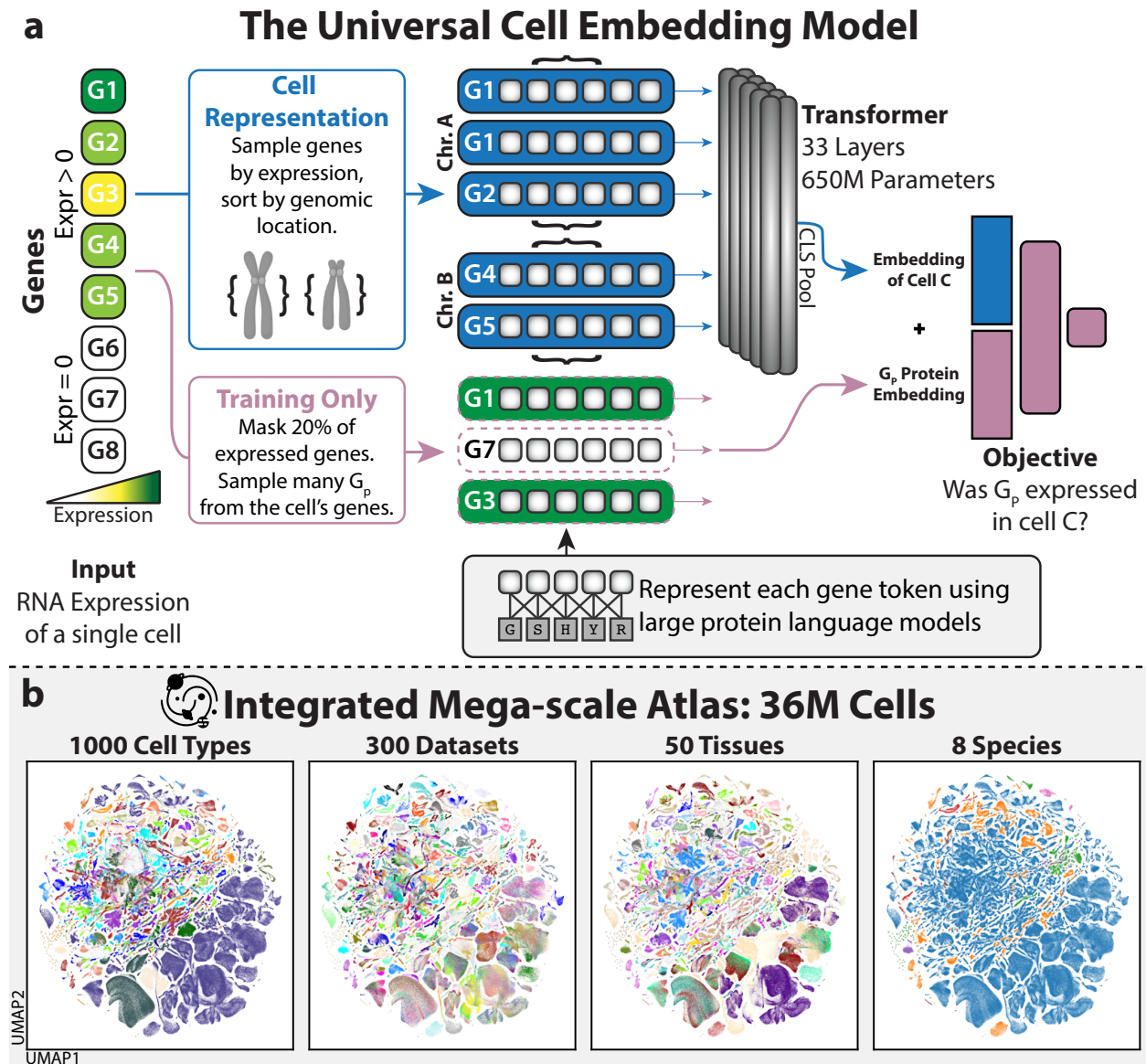


Figure 1: The Universal Cell Embedding Model is a large foundation model for single cell biology (a) Overview of the Universal Cell Embedding (UCE) model. UCE has a unique, biologically motivated representation of cells (blue) and training scheme (purple). Given the gene expression for a single cell, UCE samples with replacement genes that were expressed, weighted by their level of expression. Each gene is represented using a 'token' corresponding to its protein product. Gene tokens are represented numerically by using ESM2 protein embeddings, a 15 billion parameter protein language model that takes amino acid sequences as an input. The gene tokens are sorted by genomic location and grouped by chromosome. Chromosome groups are delineated by specific chromosome start tokens and end tokens, joined, and then passed into a transformer neural network. The embedding of the cell is determined by taking the final layer output of a special CLS token that is appended before all the other tokens. To train the UCE model, a portion of genes that were expressed are masked. The model next combines the protein embeddings corresponding to each of these genes with the embedding of the cell, and passes this joint representation through a neural network that predicts if a given gene was expressed in the cell or not. This objective function is then used to update the weights of the model. (b) UMAP visualizations of the universal cell embedding space. We apply UCE to embed 36 million cells, with more than 1,000 uniquely named cell types, from hundreds of datasets, dozens of tissues and eight species, creating an Integrated Mega-scale Atlas (IMA) spanning the universe of cell biology.

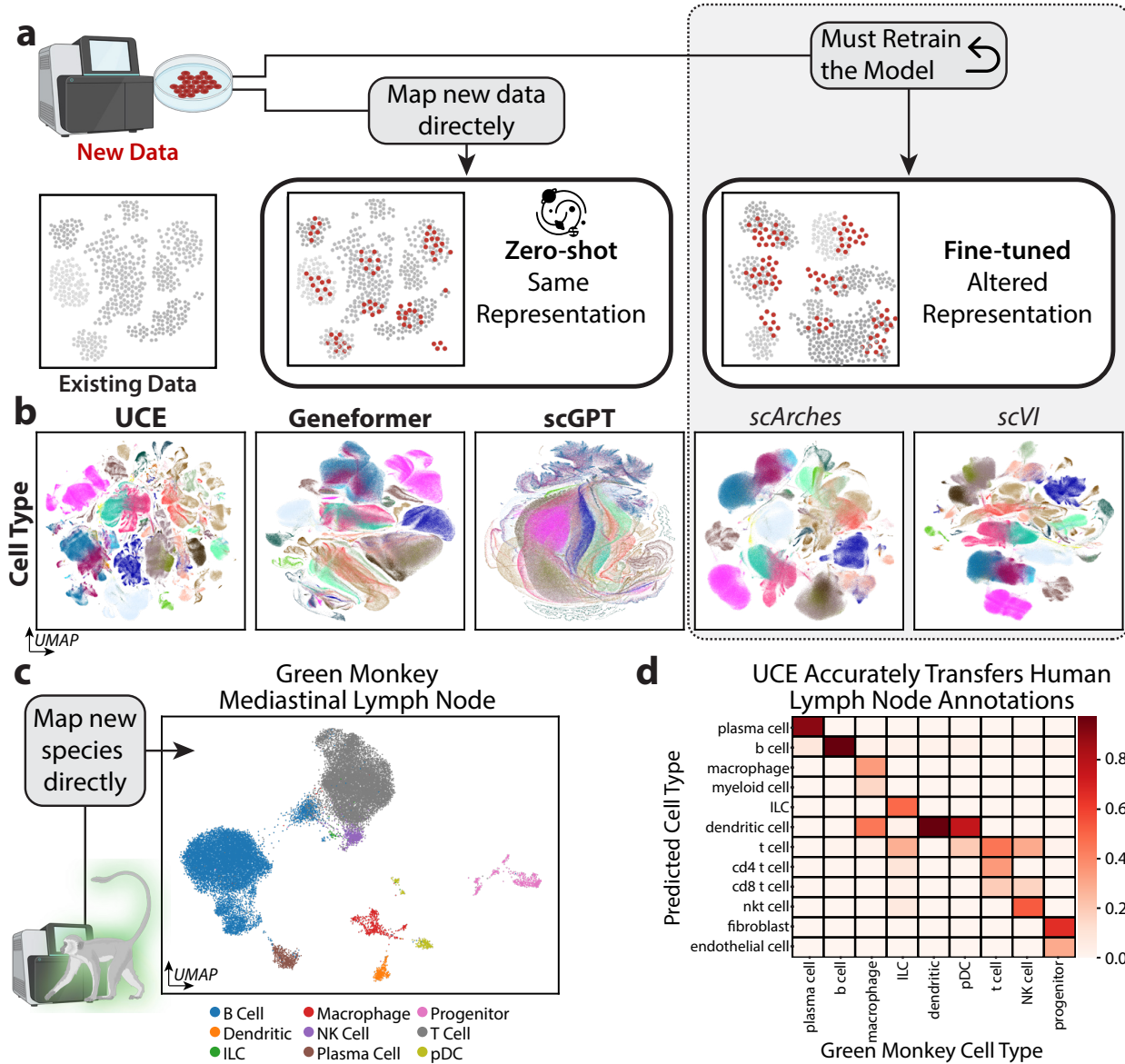


Figure 2: Zero-shot cell embedding capabilities of UCE (a) Comparison of zero-shot and fine-tuned single-cell embedding models. A zero-shot embedding model maps new data directly to the representation space of existing data, with no additional model training. In contrast, fine-tuned models must first be retrained on a given dataset, and only then can be applied on that dataset, fundamentally altering the model's representation space. (b) UMAP embeddings of UCE and other methods for *Tabula Sapiens* v1 and v2, colored by cell type. UCE zero-shot embeddings closely resemble the embeddings of fine-tuned methods scVI and scArches, demonstrating clusters that correspond to cell types, in contrast to the other zero-shot methods Geneformer and scGPT. (c) UMAP of cells from a new species, green monkey, colored by cell type. UCE is able to generate high-quality zero-shot embeddings of novel species that were never seen during training. The UCE embedding for green monkey mediastinal lymph node [39] recaptures cell type clusters. Notably, a population of B cells (blue) clusters nearby to T cells, potentially due to expression of *Cd3* (Supplementary Fig. 1). (d) Green monkey lymph node cells can be accurately annotated using the IMA. A logistic classifier is first trained to predict cell types based on UCE embeddings of human lymph node cells. The classifier is then directly applied on green monkey cells to predict the cell types. Predicted cell types have high agreement with the original cell type annotations, demonstrating that UCE can be used to transfer cell type annotations to novel species.

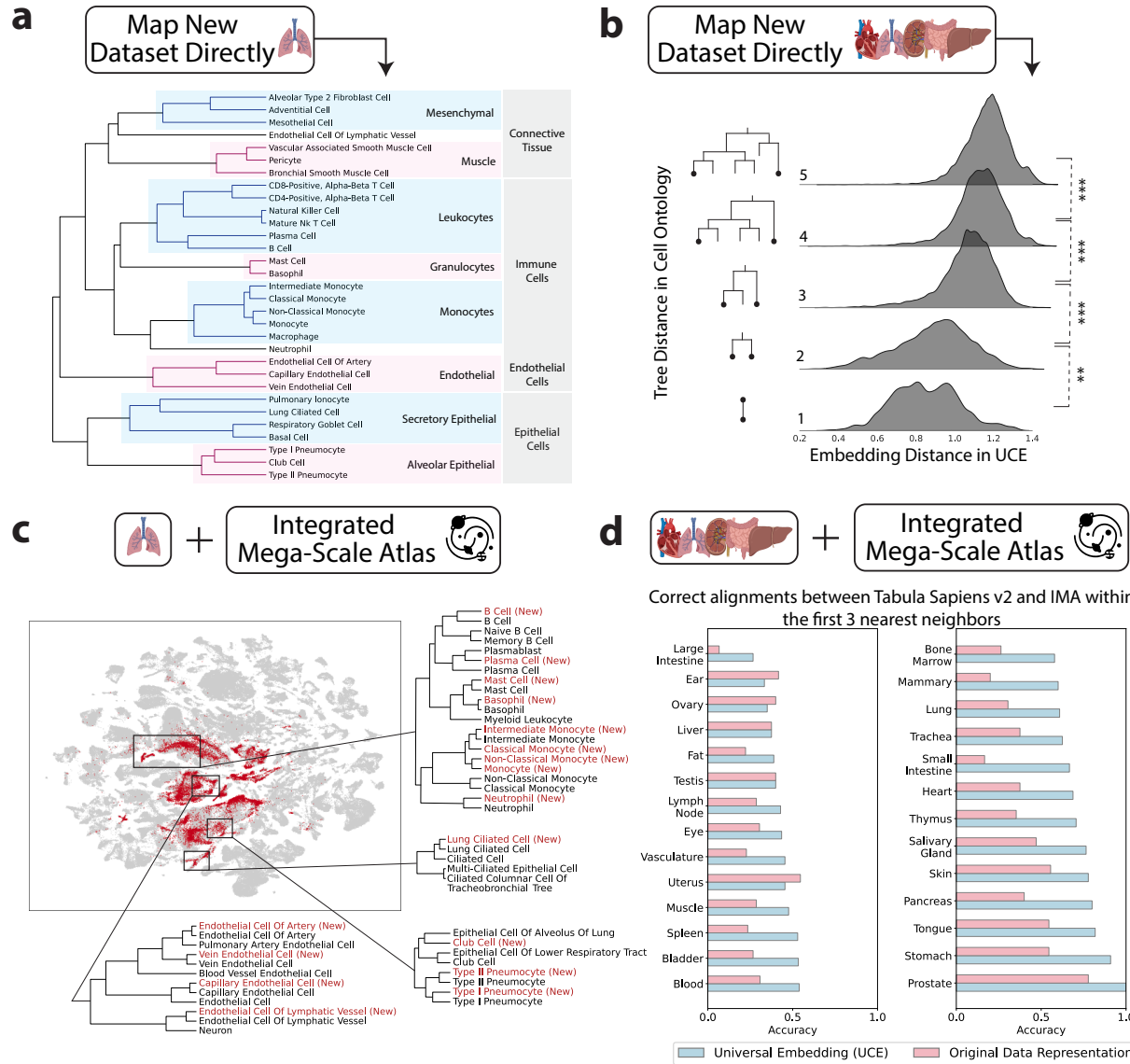


Figure 3: UCE learns meaningful organization of cell types **(a)** The UCE space generated for new, previously unseen data shows a meaningful arrangement of cell types. Lung data was used from new donors from the Tabula Sapiens Consortium. Dendrogram of hierarchical clustering of all annotated cell types in the UCE embedding space. Closely connected cell types in the dendrogram show meaningful biological relationships both at finer and coarser scale resolutions. **(b)** Evaluation of the organization of cell types in the embedding space when compared to Cell Ontology. The *x*-axis depicts the density of Euclidean distances between all pairs of cells across all tissues for these new donors from the Tabula Sapiens Consortium. The *y*-axis shows the corresponding tree distance between cell types as found in the Cell Ontology. Stars denote statistical significance, which was established using a one-sided *t*-test. **(c)** Mapping data from new donors to the Integrated Mega-scale Atlas (IMA) across multiple lung datasets. Red labels correspond to data from new donors, grey are from IMA datasets. All cell type labels from multiple datasets are displayed as-is, with no modifications or reformatting of text. Accurate alignment between the new dataset and IMA is observed at finer resolution. Four different subtypes of endothelial cells are shown to correctly map to their corresponding counterparts in the complete mega-scale atlas. In the case of lung ciliated cells, they map more closely to their matching counterpart as compared to all other ciliated cell subtypes also present in the IMA. **(d)** Quantification of cell type alignment between new dataset and IMA. Accuracy in 3-nearest centroid matches between new dataset and IMA cell types at the finest level of original annotation. Results are measured across all 27 tissues in Tabula Sapiens v2 for both the UCE space and the original gene expression space. Tissues are ordered by accuracy in the UCE space.

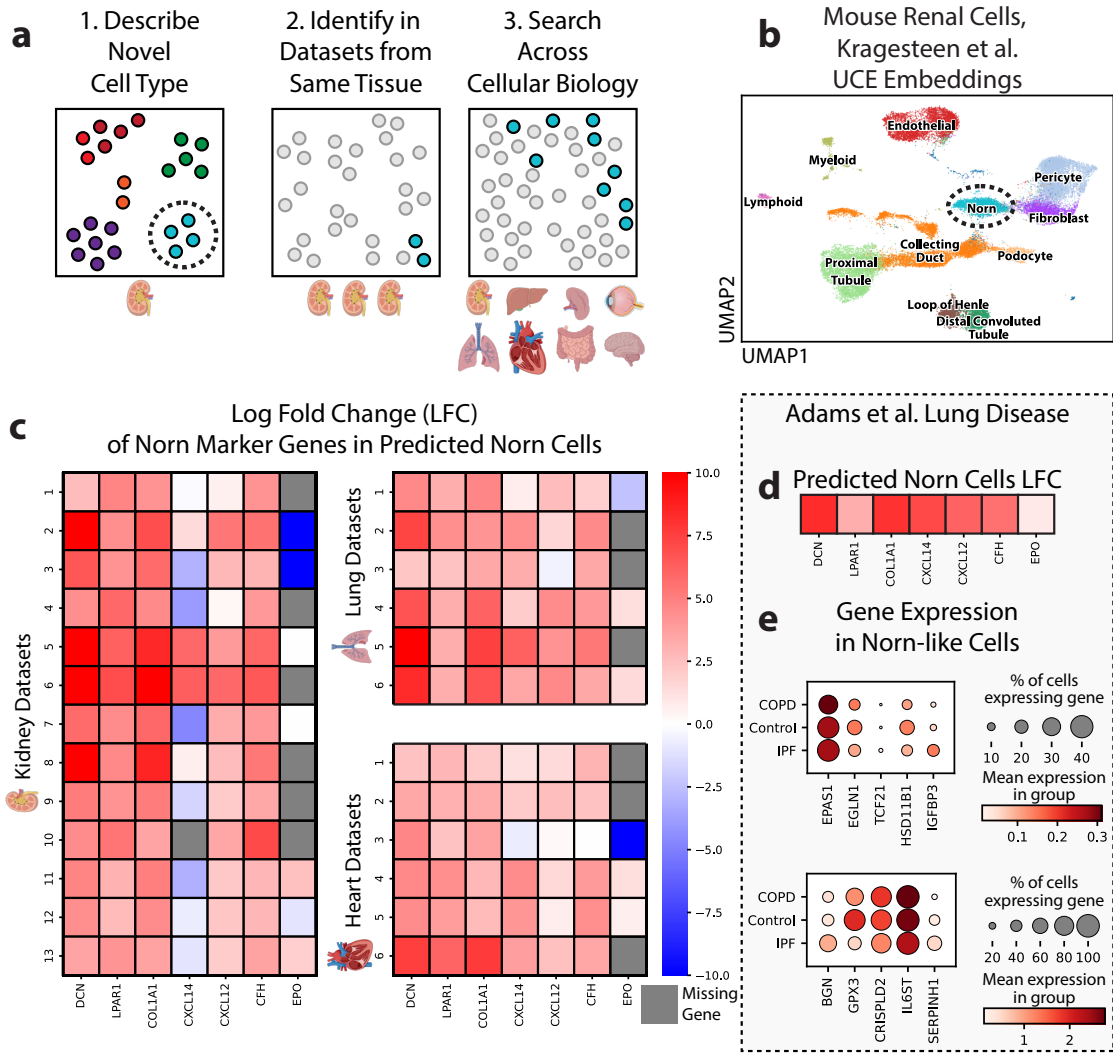


Figure 4: Norn Cell Case Study: UCE unlocks new analyses of single cell datasets **(a)** Overview of a novel single cell analysis workflow that UCE facilitates. Analysis begins with (1) the identification of a novel cell type (circled) within the embedding space, using methods such as clustering and confirmation using marker gene analysis. (2) Next, the novel cell type can be easily identified in other datasets profiled from the same tissue (for example, kidney). A simple classifier, such as a logistic classifier, is trained to predict cell types from universal cell embeddings, and is then applied to embeddings from other datasets of the same tissue (kidney), to confirm the cell type's existence and improve its characterization. (3) Finally, the same simple classifier can be applied to the embeddings of cells from any other tissue, to find cell types with similar biological functions or patterns of gene expression. **(b)** Identification of novel Norn cells in mouse kidney. UMAP visualization of zero-shot embedding of mouse renal cells from Kragsteen et al. [44]. Norn cells form a distinct cluster within the embedding space (circled). **(c)** Identification of Norn cells and Norn-like cells across tissues. A logistic classifier is trained to predict Norn cells from universal cell embeddings, and is then applied to other kidney datasets (left) and datasets from lung and heart (right). The log fold change of known Norn marker genes between cells predicted to be Norn cells and the remaining cells within each dataset is visualized. Cells which are predicted to be Norn-like preferentially express Norn markers in kidney, as well as in lung and heart. Notably, *Cxcl14* has a mixed pattern of expression among some datasets. **(d)** Cells predicted to be Norn cells within a lung disease dataset [46] express known Norn markers, as demonstrated by log fold change (LFC). **(e)** Differential gene expression in predicted Norn cells, grouped by disease status. There are significant differences in gene expression of important Norn markers and genes involved in the production of erythropoietin (*Epo*) between cells from IPF, COPD and control patients. Patients with IPF and COPD are known to have elevated levels of blood stream *Epo*, with COPD patients having greater bloodstream *Epo* levels than patients with IPF.

469 **Data availability**

470 The full list of datasets used to train UCE are in Extended Data Table 2. Most of these datasets are
471 available to download from CellXGene [36]. Tabula Sapiens v2, used for model evaluation, will
472 be made available upon publication.

473 Datasets analyzed in the paper are publicly available to download. The green monkey lung
474 and lymph node dataset is available with accession code GSE156755. The naked mole rat dataset
475 is available with accession code GSE132642. The chicken retina dataset is available with acces-
476 sion code GSE159107. The chicken heart dataset is available with accession code GSE149457.
477 The mouse kidney dataset is available with accession code GSE193321. The human lung disease
478 dataset is available with acccesion code GSE136831.

479 **Code availability**

480 UCE was written in Python using the PyTorch library. The source code is available on Github at
481 <https://github.com/snap-stanford/uce>.

482 **Acknowledgements**

483 We thank Rok Sosič, Kexin Huang, Charlotte Bunne, Hanchen Wang, Michihiro Yasunaga, Michael
484 Moor, Minkai Xu, Mika Jain, George Crowley, Maria Brbić, Jonah Cool, Nicholas Sofroniew,
485 Andrew Tolopko, Ivana Jelic, Ana-Maria Istrate and Pablo Garcia-Nieto for discussions and for
486 providing feedback on our manuscript. We acknowledge support from Robert C. Jones for help
487 with accessing and analyzing the Tabula Sapiens v2 dataset. We acknowledge support from the
488 Chan Zuckerberg Initiative, including help with accessing and processing CxG datasets. We grate-
489 fully acknowledge the support of DARPA under Nos. N660011924033 (MCS); NSF under Nos.
490 OAC-1835598 (CINES), CCF-1918940 (Expeditions), Stanford Data Science Initiative, Wu Tsai
491 Neurosciences Institute, Amazon, Genentech, GSK, Hitachi, Juniper Networks, and KDDI. Y.
492 RH. acknowledges funding support form GlaxoSmithKline. L.S. was supported by the American
493 Slovenia Education Foundation (ASEF). Icons created with BioRender.com.

494 **Author information**

495 Y.RS., Y.RH., S.Q. and J.L. conceived the study. Y.RS, Y.RH., S.Q. and J.L. performed research,
496 contributed new analytical tools, designed algorithmic frameworks, analyzed data and wrote the
497 manuscript. Y.RS. and Y.RH. performed experiments and developed the software. A.A. and L.S.
498 contributed to code and performed analyses. T.S. provided annotated data.

499 References

- 500 1. Vaishnav, E. D. *et al.* The evolution, evolvability and engineering of gene regulatory dna. *Nature* **603**, 455–463 (2022).
- 501 2. Onuchic, J. N., Luthey-Schulten, Z. & Wolynes, P. G. Theory of protein folding: the energy
502 landscape perspective. *Annual review of physical chemistry* **48**, 545–600 (1997).
- 503 3. Moris, N., Pina, C. & Arias, A. M. Transition states and cell fate decisions in epigenetic
504 landscapes. *Nature Reviews Genetics* **17**, 693–703 (2016).
- 505 4. Treutlein, B. *et al.* Reconstructing lineage hierarchies of the distal lung epithelium using
506 single-cell rna-seq. *Nature* **509**, 371–375 (2014).
- 507 5. Waddington, C. H. *The strategy of the genes* (Routledge, 1957).
- 508 6. Schaum, N. *et al.* Single-cell transcriptomics of 20 mouse organs creates a tabula muris: The
509 tabula muris consortium. *Nature* **562**, 367 (2018).
- 510 7. Regev, A. *et al.* The human cell atlas. *elife* **6**, e27041 (2017).
- 511 8. Rood, J. E., Maartens, A., Hupalowska, A., Teichmann, S. A. & Regev, A. Impact of the
512 human cell atlas on medicine. *Nature medicine* **28**, 2486–2496 (2022).
- 513 9. Tanay, A. & Regev, A. Scaling single-cell genomics from phenomenology to mechanism.
514 *Nature* **541**, 331–338 (2017).
- 515 10. Plass, M. *et al.* Cell type atlas and lineage tree of a whole complex animal by single-cell
516 transcriptomics. *Science* **360**, eaaq1723 (2018).
- 517 11. Consortium*, T. S. *et al.* The tabula sapiens: A multiple-organ, single-cell transcriptomic atlas
518 of humans. *Science* **376**, eabl4896 (2022).
- 519 12. Siletti, K. *et al.* Transcriptomic diversity of cell types across the adult human brain. *Science*
520 **382**, eadd7046 (2023).
- 521 13. Li, H. *et al.* Fly cell atlas: A single-nucleus transcriptomic atlas of the adult fruit fly. *Science*
522 **375**, eabk2432 (2022).
- 523 14. Eraslan, G., Avsec, Ž., Gagneur, J. & Theis, F. J. Deep learning: new computational modelling
524 techniques for genomics. *Nature Reviews Genetics* **20**, 389–403 (2019).
- 525 15. Lopez, R., Regier, J., Cole, M. B., Jordan, M. I. & Yosef, N. Deep generative modeling for
526 single-cell transcriptomics. *Nature methods* **15**, 1053–1058 (2018).
- 527 16. Luecken, M. D. *et al.* Benchmarking atlas-level data integration in single-cell genomics. *Na-
528 ture methods* **19**, 41–50 (2022).
- 529 17. Argelaguet, R., Cuomo, A. S., Stegle, O. & Marioni, J. C. Computational principles and
530 challenges in single-cell data integration. *Nature biotechnology* **39**, 1202–1215 (2021).
- 531 18. Lotfollahi, M. *et al.* Mapping single-cell data to reference atlases by transfer learning. *Nature*
532 **biotechnology** **40**, 121–130 (2022).

535 19. Tarashansky, A. J. *et al.* Mapping single-cell atlases throughout metazoa unravels cell type
536 evolution. *Elife* **10**, e66747 (2021).

537 20. Brown, T. *et al.* Language models are few-shot learners. *Advances in neural information*
538 *processing systems* **33**, 1877–1901 (2020).

539 21. OpenAI. Gpt-4 technical report (2023). [2303.08774](https://arxiv.org/abs/2303.08774).

540 22. Anil, R. *et al.* Palm 2 technical report. *arXiv preprint arXiv:2305.10403* (2023).

541 23. Touvron, H. *et al.* Llama: Open and efficient foundation language models. *arXiv preprint*
542 *arXiv:2302.13971* (2023).

543 24. Kirillov, A. *et al.* Segment anything. *arXiv preprint arXiv:2304.02643* (2023).

544 25. Bommasani, R. *et al.* On the opportunities and risks of foundation models. *arXiv preprint*
545 *arXiv:2108.07258* (2021).

546 26. Avsec, Ž. *et al.* Effective gene expression prediction from sequence by integrating long-range
547 interactions. *Nature methods* **18**, 1196–1203 (2021).

548 27. Rives, A. *et al.* Biological structure and function emerge from scaling unsupervised learning
549 to 250 million protein sequences. *Proceedings of the National Academy of Sciences* **118**,
550 e2016239118 (2021).

551 28. Theodoris, C. V. *et al.* Transfer learning enables predictions in network biology. *Nature* 1–9
552 (2023).

553 29. Cui, H. *et al.* scgpt: Towards building a foundation model for single-cell multi-omics using
554 generative ai. *bioRxiv* 2023–04 (2023).

555 30. Stegle, O., Teichmann, S. A. & Marioni, J. C. Computational and analytical challenges in
556 single-cell transcriptomics. *Nature Reviews Genetics* **16**, 133–145 (2015).

557 31. Quake, S. R. The cell as a bag of rna. *Trends in Genetics* **37**, 1064–1068 (2021).

558 32. Vaswani, A. *et al.* Attention is all you need. *Advances in neural information processing*
559 *systems* **30** (2017).

560 33. Lin, Z. *et al.* Evolutionary-scale prediction of atomic-level protein structure with a language
561 model. *Science* **379**, 1123–1130 (2023).

562 34. Rosen, Y. *et al.* Towards universal cell embeddings: Integrating single-cell rna-seq datasets
563 across species with saturn. *bioRxiv* (2023).

564 35. Devlin, J., Chang, M.-W., Lee, K. & Toutanova, K. Bert: Pre-training of deep bidirectional
565 transformers for language understanding. *arXiv preprint arXiv:1810.04805* (2018).

566 36. Biology, C. S.-C. *et al.* Cz cellxgene discover: A single-cell data platform for scalable explo-
567 ration, analysis and modeling of aggregated data. *bioRxiv* 2023–10 (2023).

568 37. Gordon, S., Plüddemann, A. & Martinez Estrada, F. Macrophage heterogeneity in tissues:
569 phenotypic diversity and functions. *Immunological reviews* **262**, 36–55 (2014).

570 38. Conde, C. D. *et al.* Cross-tissue immune cell analysis reveals tissue-specific features in hu-
571 mans. *Science* **376**, eabl5197 (2022).

572 39. Speranza, E. *et al.* Single-cell rna sequencing reveals sars-cov-2 infection dynamics in lungs
573 of african green monkeys. *Science translational medicine* **13**, eabe8146 (2021).

574 40. Hilton, H. G. *et al.* Single-cell transcriptomics of the naked mole-rat reveals unexpected
575 features of mammalian immunity. *PLoS Biology* **17**, e3000528 (2019).

576 41. Yamagata, M., Yan, W. & Sanes, J. R. A cell atlas of the chick retina based on single-cell
577 transcriptomics. *Elife* **10**, e63907 (2021).

578 42. Mantri, M. *et al.* Spatiotemporal single-cell rna sequencing of developing chicken hearts iden-
579 tifies interplay between cellular differentiation and morphogenesis. *Nature communications*
580 **12**, 1771 (2021).

581 43. Bard, J., Rhee, S. Y. & Ashburner, M. An ontology for cell types. *Genome biology* **6**, 1–5
582 (2005).

583 44. Kragsteen, B. K. *et al.* The transcriptional and regulatory identity of erythropoietin producing
584 cells. *Nature medicine* 1–10 (2023).

585 45. Haine, L. *et al.* Cytoprotective effects of erythropoietin: What about the lung? *Biomedicine
586 & Pharmacotherapy* **139**, 111547 (2021).

587 46. Adams, T. S. *et al.* Single-cell rna-seq reveals ectopic and aberrant lung-resident cell popula-
588 tions in idiopathic pulmonary fibrosis. *Science advances* **6**, eaba1983 (2020).

589 47. Tassiopoulos, S. *et al.* Erythropoietic response to hypoxaemia in diffuse idiopathic pulmonary
590 fibrosis, as opposed to chronic obstructive pulmonary disease. *Respiratory Medicine* **95**, 471–
591 475 (2001).

592 48. Abdel-Aziz, C., Okaily, N. & Kasem, A. Erythropoietin: role in idiopathic pulmonary fibrosis
593 revisited. *The Egyptian Journal of Chest Diseases and Tuberculosis* **69**, 716 (2020).

594 49. Tsantes, A. E. *et al.* Red cell macrocytosis in hypoxic patients with chronic obstructive
595 pulmonary disease. *Respiratory medicine* **98**, 1117–1123 (2004).

596 50. Safran, M. *et al.* The GeneCards suite. In Abugessaisa, I. & Kasukawa, T. (eds.) *Practical
597 guide to life science databases*, 27–56 (Springer Singapore, Singapore, 2021).

598 51. Stelzer, G. *et al.* The genecards suite: from gene data mining to disease genome sequence
599 analyses. *Current Protocols in Bioinformatics* **54**, 1.30.1–1.30.33 (2016).

600 52. Amaral, P. *et al.* The status of the human gene catalogue. *Nature* **622**, 41–47 (2023).

601 53. Brenner, S. Nature's gift to science (nobel lecture). *Chembiochem* **4**, 683–687 (2003).

602 54. Wolf, F. A., Angerer, P. & Theis, F. J. SCANPY: large-scale single-cell gene expression data
603 analysis. *Genome Biology* **19**, 15 (2018).